Theoretical Notes
Note 281

DNA 3928T
TN 281

ON THE STRUCTURE OF THE STEADY STATE SPACE-CHARGE-LIMITED BOUNDARY LAYER IN ONE DIMENSION

Mission Research Corporation
735 State Street
Santa Barbara, California 93101

November 1975

Topical Report for Period 1 October 1975—30 November 1975

CONTRACT No. DNA 001-76-C-0086

APPROVED FOR PUBLIC RELEASE;
DISTRIBUTION UNLIMITED.

THIS WORK SPONSORED BY THE DEFENSE NUCLEAR AGENCY
UNDER RDT&E RMSS CODE B323076464 R99QAXEB06964 H2590D.

Prepared for
Director
DEFENSE NUCLEAR AGENCY
Washington, D. C. 20305

UNCLASSIFIED

SECURITY CLASSIFICATION OF THIS PAGE *(When Data Entered)*

REPORT DOCUMENTATION PAGE

READ INSTRUCTIONS BEFORE COMPLETING FORM

1. REPORT NUMBER: DNA 3928T	2. GOVT ACCESSION NO.
3. RECIPIENT'S CATALOG NUMBER	
4. TITLE *(and Subtitle)*: ON THE STRUCTURE OF THE STEADY STATE SPACE-CHARGE-LIMITED BOUNDARY LAYER IN ONE DIMENSION	5. TYPE OF REPORT & PERIOD COVERED: Topical Report for Period 1 Oct 75–30 Nov 75
	6. PERFORMING ORG. REPORT NUMBER: MRC-R-240
7. AUTHOR(s): Neal J. Carron, Conrad L. Longmire	8. CONTRACT OR GRANT NUMBER(s): DNA 001-76-C-0086
9. PERFORMING ORGANIZATION NAME AND ADDRESS: Mission Research Corporation, 735 State Street, Santa Barbara, California 93101	10. PROGRAM ELEMENT, PROJECT, TASK AREA & WORK UNIT NUMBERS: Subtask R99QAXEB069-64
11. CONTROLLING OFFICE NAME AND ADDRESS: Director, Defense Nuclear Agency, Washington, D.C. 20305	12. REPORT DATE: November 1975
	13. NUMBER OF PAGES: 50
14. MONITORING AGENCY NAME & ADDRESS *(if different from Controlling Office)*	15. SECURITY CLASS *(of this report)*: UNCLASSIFIED
	15a. DECLASSIFICATION DOWNGRADING SCHEDULE

16. DISTRIBUTION STATEMENT *(of this Report)*

Approved for public release; distribution unlimited.

17. DISTRIBUTION STATEMENT *(of the abstract entered in Block 20, if different from Report)*

18. SUPPLEMENTARY NOTES

This work sponsored by the Defense Nuclear Agency under RDT&E Code B323076464 R99QAXEB06964 H2590D.

19. KEY WORDS *(Continue on reverse side if necessary and identify by block number)*

SGEMP
X-ray Photoemission
Space-Charge Limiting
Boundary Layer
Steady State

20. ABSTRACT *(Continue on reverse side if necessary and identify by block number)*

We study the external SGEMP boundary layer in one Cartesian dimension in the steady-state limit. Dimensional arguments backed by explicit calculations show the surface charge density to be independent of the electron charge, and show that the characteristic potential and dipole moment of the layer are practically independent of fluence. The general equation of motion is shown to imply that the electrostatic energy density is everywhere twice the density of kinetic energy stored in the normal component of electron motion.

DD FORM 1 JAN 73 1473 EDITION OF 1 NOV 65 IS OBSOLETE

UNCLASSIFIED

SECURITY CLASSIFICATION OF THIS PAGE *(When Data Entered)*

20. ABSTRACT (Continued)

Detailed solutions are given for several electron energy spectra including an exponential energy spectrum with a coseΘ angular emission spectrum. Estimates are given for the times at which the steady-state solution should be applicable.

TABLE OF CONTENTS

LIST OF ILLUSTRATIONS

SECTION 1
INTRODUCTION

This report is the first in a series of reports to appear on analytic studies of general SGEMP phenomena. They are intended to investigate the physical phenomena involved in the generation of skin currents, surface charge densities, and electromagnetic fields, and in coupling mechanisms to internal circuitry. It is hoped to provide at least a qualitative and preferably a quantitative understanding on theoretical grounds, to provide a physical understanding of the various computer code results obtained to date, and to help in predicting expected order of magnitude effects on real three-dimensional targets.

The spirit of our approach is to adopt Fermi's philosophy that "one should never do a (detailed) calculation until one already knows what the answer is." We wish to outline the basic physics of SGEMP phenomena so that we have a sound theoretical framework in terms of which we can understand the more detailed computer results.

The present report deals with the steady state electron emission boundary layer. In the future we hope to study the time-dependent transient build-up of the layer.

If we think of the chronological sequence of events occurring in a typical SGEMP problem, we have first the arriving X rays illuminating the exposed satellite surfaces and ejecting photoelectrons. These electrons constitute an electric current which is the basic driver of Maxwell's

equations. The exposed surface is left positive and this positive charge flows away on the satellite surface producing the skin currents.

The photoelectrons above the positive surface produce a strong normal electric field. At relatively high fluences, large numbers of low-energy electrons are held back by this field and congregate near the surface, producing a boundary layer of relatively dense charged plasma. Of the subsequently emitted electrons, only the more energetic ones can penetrate the potential of this layer and move through space around the satellite.

Hence the boundary layer greatly affects electrons that penetrate it by reducing their energy. Also, the layer constitutes a dipole layer producing its own external field. In addition, the structure of the layer near the edges of exposed surfaces will determine how the electrons flow around the edges, and may help in understanding the surge of replacement current around the sides.

The boundary layer structure is a function of the X-ray fluence, time history, and energy spectrum, and the photoelectric yield of the target. Its thickness can be less than a millimeter for high fluences and soft spectra, and larger than the satellite dimensions for hard spectra and low fluences so that it hardly exists. This wide range of thicknesses makes it difficult to handle by a single technique in SGEMP codes designed for a wide range of fluences and spectra.

In this report we study the structure of the boundary layer in the steady-state approximation and in one dimension. In this case the problem can be reduced to quadratures, and so solved completely. Previous workers have investigated various aspects of this problem[1,2,3]. Here we consolidate these previous results from a unified point of view and present some new results of interest.

SECTION 2
CHARACTERISTIC DIMENSIONS

Figure 1 shows a sketch of the relevant geometry. The z direction is normal to the surface. The X rays are incident from above in the normal direction. Electrons are ejected upward with some angle and energy distribution. In the steady state, the electron number density n(z), electric field E(z), and potential $\Phi(z)$ will all be single valued functions of z.

Let w_1 be a characteristic energy of the emitted electrons, and

$$v_1 = \sqrt{2\, w_1/m} \ , \tag{1}$$

be a characteristic velocity. The electron number density at the surface, n(0), which includes both emitted and returning electrons, defines a plasma frequency ω_p by

$$\omega_p = \sqrt{\frac{4\pi e^2}{m}\, n(0)} \ . \tag{2}$$

The energy w_1 defines the characteristic dimension ℓ_D, the Debye length, by

$$\ell_D = \sqrt{\frac{w_1}{4\pi e^2 n(0)}} = \frac{v_1}{\sqrt{2}\,\omega_p} \ . \tag{3}$$

This is the distance over which n, E, and Φ vary appreciably.

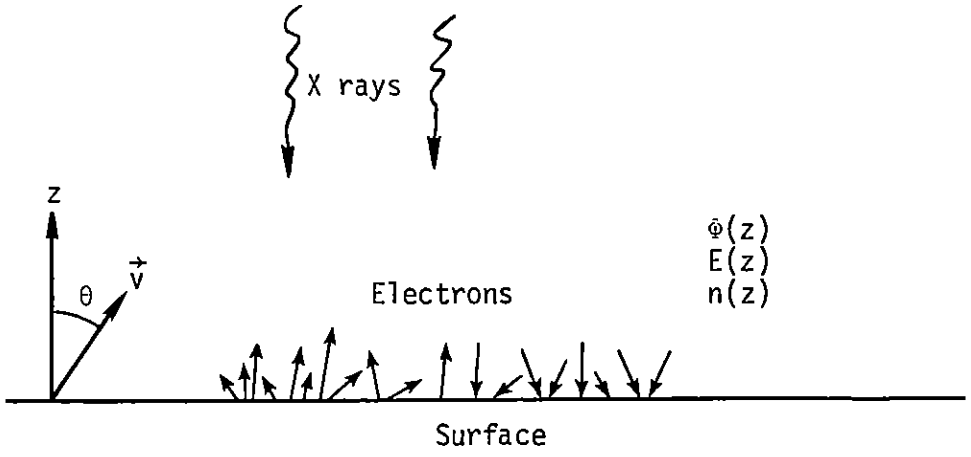

Figure 1. Sketch of geometry.

The other dimensional unit of distance is e^2/w_1. But this is not a plasma quantity and is at any rate exceedingly small. Since $e^2 = 1.44 \times 10^{-10}$ keV cm, and w_1 is a few keV, $e^2/w_1 \lesssim 10^{-10}$ cm, and is not a dimension of concern. It is the distance of closest approach of two electrons with relative energy w_1.

The average distance between electrons is

$$n(0)^{-1/3} = \left(4\pi \ell_D^2 \frac{e^2}{w_1}\right)^{1/3} >> \frac{e^2}{w_1} . \qquad (4)$$

If electrons are ejected at a rate r_0 (electrons/cm^2/sec), which is the product of the material yield Y(elecs/cal) and the X-ray flux $d\phi/dt$ (calories/cm^2/sec),

$$r_0 = Y \frac{d\phi}{dt} \quad \frac{\text{electrons}}{\text{cm}^2 \text{ sec}} , \qquad (5)$$

then the number density at the surface will be on the order of

$$n(0) \sim \frac{2r_0}{v_1} \text{ elecs/cm}^3 , \tag{6}$$

and the total number of electrons will be on the order of

$$N_s \sim n(0)\ell_D \sim \sqrt{\frac{mv_1 r_0}{4\pi e^2}} \text{ elecs/cm}^2 . \tag{7}$$

The surface charge density σ will be

$$\sigma = eN_s \sim \sqrt{mv_1 r_0/4\pi} \text{ esu/cm}^2 , \tag{8}$$

and is, curiously, independent of the electron charge. If e were not a constant, for example if it were larger, each ejected electron would leave behind more charge, but the electrons would return more rapidly to the surface, so that in the steady state σ does not depend on e.

Likewise the surface electric field, E(0), will be of order

$$E(0) = 4\pi\sigma \sim \sqrt{4\pi m v_1 r_0} \text{ esu} , \tag{9}$$

and is also independent of e. Both σ and E(0) increase as $r_0^{1/2}$ and therefore with the square root of the fluence.

The potential Φ_1 of the surface relative to a distant point will be of order

$$\Phi_1 \sim E(0)\ell_D \sim 4\pi e n(0)\ell_D^2 = \frac{w_1}{e} . \tag{10}$$

Thus the characteristic potential depends only on the electron energy spectrum, and is independent of fluence.

The dipole moment per unit area of the boundary layer will be of order

$$P \sim eN_s\ell_D = \sigma\ell_D \sim \frac{w_1}{4\pi e} \text{ esu-cm/cm}^2 , \tag{11}$$

also independent of fluence. Thus one might expect that the quasi-static field produced by the boundary layer's dipole moment will become relatively less and less important as fluence increases since this field is independent of fluence whereas other sources of dynamical fields increase with fluence.

The kinetic energy stored in the moving electrons will be of order

$$K \sim w_1 N_s \sim \frac{1}{2} m v_1^2 \sqrt{\frac{m v_1 r_0}{4\pi e^2}} \quad \text{ergs/cm}^2 \ , \tag{12}$$

and the energy stored in the electric field will be of order

$$U \sim \frac{E(0)^2}{8\pi} \ell_D \sim K \quad \text{ergs/cm}^2 \ . \tag{13}$$

Later we show that general principles actually imply that U = 2K exactly for the normal component of motion. Subsequent detailed calculations in this report confirm all of the above dimensional arguments.

TIME CONSIDERATIONS

The characteristic turn around time for an electron trajectory will be of order

$$t_1 \sim \frac{\ell_D}{v_1} \sim \frac{1}{\omega_p} \sim \sqrt{\frac{m v_1}{8\pi e^2 r_0}} \ , \tag{14}$$

We estimate t_1 when w_1 = 2 keV, Y = 1.25 x 10^{13} elec/cal (2 keV blackbody on Aluminum), and the X-ray pulse FWHM is 3 shakes. Then

$$t_1 \sim 1.4 \sqrt{\frac{10^{-3}}{\phi(\text{cal/cm}^2)}} \quad \text{nanosec} \ , \tag{15}$$

where ϕ is the X-ray fluence, and we have approximated $d\phi/dt$ in Equation 5 by its average value $\phi/2$ FWHM. Hence for fluences above 10^{-3} cal/cm^2, $t_1 \lesssim 1$ ns. This indicates that the steady-state solutions discussed in this

report will be applicable when the X-ray flux is not changing appreciably over times of order 1 ns at 10^{-3} cal/cm^2 or of order 0.1 ns at 10^{-1} cal/cm^2.

The steady-state solution should begin to become a good approximation when the total number of electrons ejected

$$N(t) = Y \int_0^t \frac{d\phi}{dt}\, dt \quad \text{elecs/cm}^2 \ , \tag{16}$$

is larger than the steady-state number

$$N_s(t) \sim \sqrt{\frac{mv_1}{4\pi e^2}\, Y\, \frac{d\phi}{dt}\,(t)} \ , \tag{17}$$

from Equation 7. Assuming a triangular time pulse with a rise time t_{rise}, and a full pulse width T = 2 FWHM,

$$\frac{d\phi}{dt} = 2\,\frac{\phi}{T}\,\frac{t}{t_{rise}} \ , \quad 0 < t \le t_{rise} \ , \tag{18}$$

for the rising portion of the pulse. Using 18 and equating 16 and 17 one obtains

$$t^3 = t_{rise}\,\frac{mv_1}{2\pi e^2}\,\frac{T}{Y\phi} \ , \tag{19}$$

or

$$t = 2.28\left[\sqrt{w_1(\text{keV})}\; t_{rise}(\text{shakes})\; T(\text{shakes})\; \frac{10^{13}}{Y}\,\frac{10^{-3}}{\phi}\right]^{1/3} \text{ns} \ . \tag{20}$$

Using Y = 1.25 x 10^{13} elec/cal, T = 6 shakes, t_{rise} = 1 shake, w_1 = 2 keV,

$$t = 4.3\left(\frac{10^{-3}}{\phi(\text{cal/cm}^2)}\right)^{1/3} \text{nanosec} \ , \tag{21}$$

which varies from 10 to 1 ns as ϕ increases from 10^{-4} to 10^{-1} cal/cm^2.

SECTION 3

THE RELATION BETWEEN EMISSION ANGULAR DISTRIBUTION AND NORMAL ENERGY DISTRIBUTION

In our one-dimensional problem only the normal component of motion is affected. Electrons are ejected with some energy and angle distribution $d^2n/dwd\Omega$ (electrons/cm^2 sec keV ster), but the dynamics influences only the z component of velocity v_z. The emission energy distribution is

$$\frac{dn}{dw} = \int_{2\pi} \frac{d^2n}{dwd\Omega}\, d\Omega \quad \frac{\text{electrons}}{cm^2 \text{ sec keV}} \quad , \tag{22}$$

with the integral taken over the emission hemisphere, and the three-dimensional velocity distribution is

$$\frac{d^3n}{d^3v} = \frac{m}{v}\frac{d^2n}{dwd\Omega} \quad \frac{\text{electrons}}{cm^2 \text{ sec } (cm/sec)^3} \quad . \tag{23}$$

The z component of velocity is distributed according to

$$\begin{aligned} \frac{dn}{dv_z} &= \int_{-\infty}^{\infty} dv_x dv_y \frac{d^3n}{d^3v} \\ &= m \int_0^{\infty} dv_\perp \frac{v_\perp}{v} \int_0^{2\pi} \frac{d^2n}{dwd\Omega}\, d\phi \quad , \end{aligned} \tag{24}$$

where

$$v_\perp = \sqrt{v_x^2 + v_y^2} = \sqrt{v^2 - v_z^2} \quad , \tag{25}$$

and ϕ is the azimuth angle. We now assume the emission spectrum factorizes into energy and angle parts,

$$\frac{d^2n}{dwd\Omega} = \frac{dn}{dw}\, g(\theta,\phi) \ , \tag{26}$$

where θ is the polar angle from the normal as in Figure 1. Then using $dw = mv_\perp dv_\perp$, valid when v_z is held fixed,

$$\frac{dn}{dv_z} = \int_{w_z}^{\infty} \frac{dw}{\sqrt{2w/m}} \frac{dn}{dw} \int_0^{2\pi} g\, d\phi \ , \tag{27}$$

where

$$w_z = \frac{1}{2} m v_z^2 \ , \tag{28}$$

is the normal component of energy. We now assume the emission is a $\cos\theta$ distribution,

$$g(\theta,\phi) = \frac{1}{\pi} \cos\theta = \frac{v_z}{\pi v} \ ,$$

which is close to the experimental facts and to the distribution predicted by the code QUICKE2. In this case, Equation 27 yields for the distribution of w_z,

$$\frac{dn}{dw_z} = \int_{w_z}^{\infty} \frac{dw}{w} \frac{dn}{dw} \left(\frac{\text{electrons}}{\text{cm}^2 \text{ sec keV}} \right) . \tag{29}$$

The following several examples of energy distributions dn/dw with a $\cos\theta$ angle distribution and the resulting dn/dw_z are instructive.

1. Monoenergetic

$$\frac{dn}{dw} = r_0 \delta(w - w_1) \ , \tag{30}$$

$$\frac{dn}{dw_z} = \frac{r_0}{w_1}\,\theta(w_1 - w_z)\ , \tag{31}$$

where $\theta(x)$ is the unit step function $\theta(x) = 1$ if $x > 0$, $\theta(x) = 0$ if $x < 0$. A monoenergetic $\cos\theta$ distribution produces a constant w_z distribution.

2. Constant

$$\frac{dn}{dw} = \frac{r_0}{w_1}\,\theta(w_1 - w)\ , \tag{32}$$

$$\frac{dn}{dw_z} = \frac{r_0}{w_1}\,\ell n\,\frac{w_1}{w_z} \quad , \quad 0 < w_z < w_1\ , \tag{33}$$

3. Linear Increase

$$\frac{dn}{dw} = \frac{2r_0 w}{w_1^2} \quad , \quad 0 < w < w_1\ , \tag{34}$$

$$\frac{dn}{dw_z} = \frac{2r_0}{w_1^2}\,(w_1 - w_z) \quad , \quad 0 < w_z < w_1\ . \tag{35}$$

A linearly increasing $\cos\theta$ distribution produces a linearly decreasing w_z distribution.

4. Linear Decrease

$$\frac{dn}{dw} = \frac{2r_0}{w_1^2}\,(w_1 - w) \quad , \quad 0 < w < w_1\ , \tag{36}$$

$$\frac{dn}{dw_z} = \frac{2r_0}{w_1^2}\left[w_1\,\ell n\,\frac{w_1}{w_z} + w_z - w_1\right] \quad , \quad 0 < w_z < w_1\ , \tag{37}$$

5. Exponential

$$\frac{dn}{dw} = \frac{r_0}{w_1}\,e^{-w/w_1}\ , \tag{38}$$

$$\frac{dn}{dw_z} = \frac{r_0}{w_1} \int_{w_z/w_1}^{\infty} dx \, \frac{e^{-x}}{x}$$

$$= \frac{r_0}{w_1} E_1(w_z/w_1) \quad , \tag{39}$$

where $E_1(x)$ is the exponential integral. This case is of interest because actual electron energy spectra when blackbody photon sources are incident are very nearly exponential[4]. Note dn/dw_z diverges logarithmically as $w_z \to 0$.

6. Linear Times Exponential

$$\frac{dn}{dw} = \frac{r_0}{w_1^2} w \, e^{-w/w_1} \quad , \tag{40}$$

$$\frac{dn}{dw_z} = \frac{r_0}{w_1} e^{-w_z/w_1} \quad . \tag{41}$$

Here the z "component" of energy is exponentially distributed. The energy spectrum 40 is essentially an exponential with the low-energy electrons deleted. Hence, comparing results for cases 5 and 6 above will indicate the effect of the low-energy electrons. For example we shall find that the slope of the charge density, $d\rho/dz$, at $z = 0$ diverges for case 5 but is finite for case 6. Equation 40 is also the emission energy spectrum for particles of a Maxwellian gas escaping through a small hole.

These six energy spectra are sketched in Figure 2. The $\cos\theta$ distribution always enhances the low energy end of dn/dw_z. In particular dn/dw_z diverges logarithmically as $w_z \to 0$ if dn/dw is non-zero as $w \to 0$.

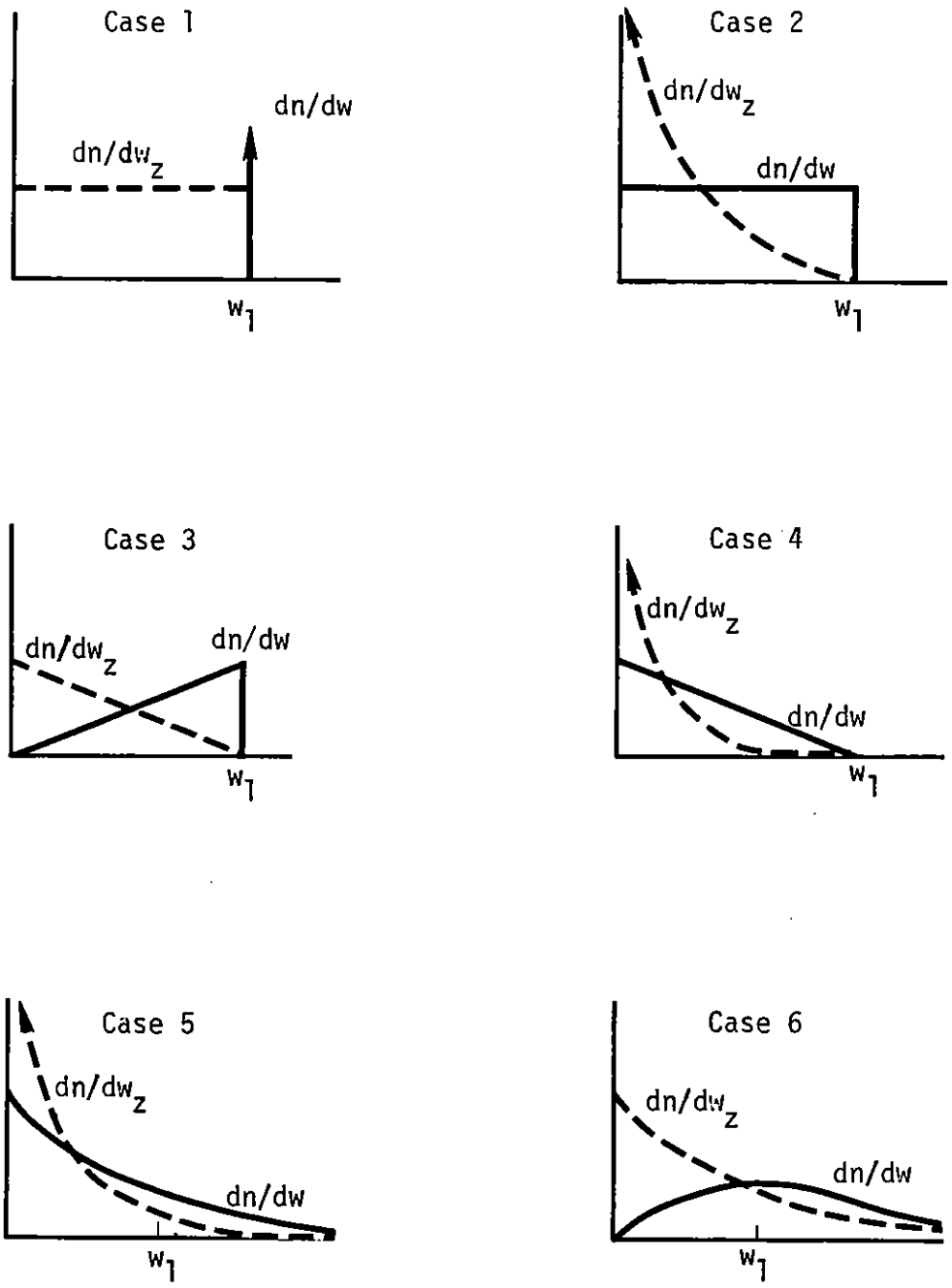

Figure 2. Normal energy distributions from several cosθ distributions.

SECTION 4

SOLUTION FOR BOLTZMANN DISTRIBUTION FUNCTION

The problem may be set up by solving for the scalar potential Φ from Poisson's equation

$$\nabla^2\Phi = \frac{\partial^2\Phi}{\partial z^2} = - 4\pi\rho(z) \ , \tag{42}$$

and for the particle motion from the time independent Boltzmann equation for the distribution function f

$$\vec{v} \cdot \vec{\nabla} f - \frac{e}{m} \vec{E} \cdot \vec{\nabla}_v f = v_z \frac{\partial f}{\partial z} - \frac{e}{m} E(z) \frac{\partial f}{\partial v_z} = 0 \ , \tag{43}$$

where

$$E(z) = - \frac{\partial\Phi}{\partial z} \ , \tag{44}$$

and

$$\rho(z) = - e \int d^3 \vec{v} f \ . \tag{45}$$

By dividing 43 by $-ev_z E(z)$, and using $E(z)dz = -d\Phi$, and $dw_z = mv_z dv_z$, we obtain

$$\frac{\partial f}{e\partial\Phi} + \frac{\partial f}{\partial w_z} = 0 \ , \tag{46}$$

the general solution to which is any function of $w_z - e\Phi$,

$$f = f(w_z - e\Phi) \ . \tag{47}$$

The correct function to use in 47 is obtained by matching the boundary condition on f at the emission surface, obtained as follows.

The differential rate of emitting electrons is $f(z = 0)v_z$ and is given by Equation 23,

$$f(z = 0)v_z = \frac{d^3n}{d^3v} = \frac{m}{v}\frac{d^2n}{dwd\Omega}\frac{\text{elecs}}{\text{cm}^2\ \text{sec}\ (\text{cm/sec})^3} . \qquad (48)$$

Again assuming a $\cos\theta$ distribution, we have

$$f(z = 0) = \frac{m}{vv_z}\frac{dn}{dw}\frac{1}{\pi}\cos\theta$$

$$= \frac{m}{\pi v^2}\frac{dn}{dw}$$

$$= \frac{m^2}{2\pi}\frac{1}{w}\frac{dn}{dw} . \qquad (49)$$

The distribution of v_z is obtained by integrating out the v_x and v_y dependence to the one-dimensional distribution function

$$f_1(z,v_z) = \int dv_x dv_y\ f(z,\vec{v}) , \qquad (50)$$

so that

$$f_1(z = 0,v_z) = \int dv_x dv_y\ f(0,v)$$

$$= m\int_{w_z}^{\infty}\frac{dw}{w}\frac{dn}{dw} . \qquad (51)$$

Since Equation 46 also holds for f_1, 47 implies, with the help of 29,

$$f_1(z,v_z) = 2m\int_{w_z - e\Phi}\frac{dw}{w}\frac{dn}{dw}$$

$$= 2m\frac{dn}{dw_z}(w_z - e\Phi) . \qquad (52)$$

3.

We have multiplied by a factor of 2 in Equation 52 to account for the returning electrons in the steady state, and have taken $\Phi(z = 0) = 0$.

The charge density 45 is then

$$\rho(z) = - e \int_0^\infty dv_z \, f_1$$

$$= - e \sqrt{2m} \int_{-e\Phi}^\infty \frac{dw_z}{\sqrt{w_z + e\Phi}} \frac{dn}{dw_z} \tag{53}$$

$$= \rho(\Phi) \ .$$

An alternate expression can be obtained with $\frac{dn}{dw}$ by using the first line of Equation 52 and interchanging the order of integrations on v_z and w,

$$\rho(z) = - 2e \sqrt{2m} \int_{-e\Phi}^\infty \frac{dw}{w} \sqrt{w + e\Phi} \frac{dn}{dw} \ . \tag{54}$$

These arguments and some in the following section are similar to those of Higgins[3].

SECTION 5

SOLUTION OF POISSON EQUATION

With ρ given by 53 or 54 as a function of Φ, Poisson's equation is

$$\frac{\partial^2 \Phi}{\partial z^2} = -4\pi\rho(\Phi)$$

$$= \frac{1}{2}\frac{\partial}{\partial \Phi}\left(\frac{\partial \phi}{\partial z}\right)^2 \qquad (55)$$

so that

$$E = -\partial\Phi/\partial z$$

$$= \left\{-8\pi \int_{\Phi(a)}^{\Phi(z)} \rho(\Phi')d\Phi' + E(a)^2\right\}^{1/2}, \qquad (56)$$

is the electric field as a function of $\Phi(z)$. Here $E(a)$ is an integration constant, the field at any point $z = a$. If the emission energy spectrum has a maximum energy $w_z(\max)$, the boundary layer will have a maximum extent z_{max} and the maximum potential will be $\Phi_{max} = -w_z(\max)/e = \phi(z_{max})$, and $E(z_{max}) = 0$. Then the electric field will be

$$E(z) = \left\{-8\pi \int_{\Phi_{max}}^{\Phi(z)} \rho(\Phi')d\Phi'\right\}^{1/2}. \qquad (57)$$

If the emission energy spectrum has electrons of arbitrarily high energy, then $z_{max} = \infty$, $E(\infty) = 0$, and Equation 57 will still hold with $\Phi_{max} = -\infty$. Integrating once again,

$$z = -\int_0^{\Phi} d\Phi' \left\{ -8\pi \int_{\Phi_{max}}^{\Phi'} \rho(\Phi'')d\Phi'' \right\}^{-1/2} . \qquad (58)$$

The inverse of 58 gives $\Phi(z)$ and completely solves the one-dimensional steady-state problem. This solution was given by Hale for several spectra[2].

Equations 57 and 53 give for the electric field at the surface

$$E(0)^2 = 8\pi e\sqrt{2m} \int_{\Phi_{max}}^{0} d\Phi' \int_{-e\Phi'}^{w_z(max)} \frac{dw_z}{\sqrt{w_z + e\Phi'}} \frac{dn}{dw_z} . \qquad (59)$$

Interchanging the orders of integration permits the Φ' integral to be done. Let w_1 be a characteristic energy in the emission spectrum. Then we find

$$E(0)^2 = 16\pi\sqrt{2mw_1}\, r_0 \int_0^{w_z(max)} dw_z \sqrt{\frac{w_z}{w_1}} \frac{1}{r_0} \frac{dn}{dw_z} . \qquad (60)$$

The integral is a dimensionless function of the emission spectrum, and hence Equation 60 confirms our dimensional arguments in Equations 9, 8, and 7, for $E(0)$, $\sigma = E(0)/4\pi$, and $N_s = \sigma/e$.

The dipole moment per unit area $P(z)$ contributed by all electrons out to a distance z is

$$P(z) = \int_0^z z\rho(z)dz . \qquad (61)$$

Using $\partial E/\partial z = 4\pi\rho$ and integrating by parts, this can be expressed as

$$P(z) = \frac{1}{4\pi} [\Phi(z) + zE(z)] . \qquad (62)$$

If the emission spectrum has a maximum energy $w_z(max)$, the total dipole moment will be

$$P = P(z_{max}) = \frac{\Phi_{max}}{4\pi} = -\frac{w_z(max)}{4\pi e} \quad , \tag{63}$$

independent of fluence as in Equation 11. If there is no maximum energy, $P(z)$ may diverge as $z \to \infty$. This occurs for cases 5 and 6, and $P(z)$ is only weakly dependent on fluence when $z >> \ell_D$.

SECTION 6

ENERGY CONSIDERATIONS

The equations of motion for the electrons can be written in the form of a conservation law by introducing the momentum densities $\vec{\pi}$ and $\vec{G}$, and momentum flow tensors P_{ij} and T_{ij} of the particles and fields[5]. Then these equations read

$$\frac{\partial}{\partial t}(\pi_i + G_i) + \frac{\partial}{\partial x_j}(P_{ij} + T_{ij}) = 0 , \tag{64}$$

where

$$\pi_i = \int m v_i f d^3v$$

$$P_{ij} = \int m v_i v_j f d^3v$$

$$G_i = \frac{1}{4\pi c}(\vec{E} \times \vec{B})_i$$

$$T_{ij} = \frac{1}{4\pi}\left[\frac{1}{2}(E^2 + B^2)\delta_{ij} - (E_i E_j + B_i B_j)\right] .$$

In steady state one dimension, the time derivative and x and y derivatives in 64 vanish, leaving

$$\frac{\partial}{\partial z}(P_{i3} + T_{i3}) = 0 , \tag{65}$$

so that $P_{i3} + T_{i3}$ is independent of z. In the present problem, $E_i = E\delta_{i3}$, $\vec{B} = 0$, so the i = 3 component of 65 reads

$$\int m v_z^2 f d^3v - \frac{E^2}{8\pi} = \text{constant} . \tag{66}$$

At large z, both terms on the left hand side of 66 separately vanish, so the constant is zero. The energy density stored in the electrostatic field is

$$u_E = \frac{E^2}{8\pi} , \tag{67}$$

and the density of z component of kinetic energy, k_z, is

$$k_z = \int \frac{1}{2} m v_z^2 f \, d^3v , \tag{68}$$

so that 66 implies

$$u_E = 2 \, k_z . \tag{69}$$

The electrostatic energy density is everywhere twice the z kinetic energy density. With a $\cos\theta$ emission distribution, f is independent of angles so the x and y contributions to the kinetic energy, k_x, and k_y, are each equal to k_z. The total kinetic energy density is

$$\begin{aligned} k &= k_x + k_y + k_z \\ &= \int \frac{1}{2} m v^2 f \, d^3v \\ &= 3 \, k_z , \end{aligned} \tag{70}$$

and Equation 69 implies

$$u_E = \frac{2}{3} k . \tag{71}$$

Integrating on z, the total stored electrostatic energy

$$U_E = \int_0^{z_{max}} u_E(z) \, dz ,$$

and the total stored kinetic energy

$$K = \int_0^{z_{max}} k(z)\, dz \quad ,$$

are related by

$$U_E = \frac{2}{3} K \quad . \tag{72}$$

SECTION 7

SEVERAL EXAMPLES

In this section we collect some formulas and graphs for four interesting examples.

Example 1 - Monoenergetic Normal Emission

Electrons are emitted normally at r_0 elecs/cm^2/sec all with energy $w_1 = \frac{1}{2} mv_1^2$. This case was first discussed by Karzas and Latter[1].

The number density at z = 0 is

$$n(0) = 2r_0/v_1 \ , \tag{73}$$

and the Debye length, Equation 3, is

$$\ell_D = \sqrt{\frac{w_1 v_1}{8\pi e^2 r_0}} \ . \tag{74}$$

The maximum distance the electrons travel is

$$z_{max} = \frac{2}{3} \ell_D \ . \tag{75}$$

The electric field at the surface is

$$E(0) = 4\sqrt{\pi m r_0 v_1}$$

$$= \frac{4}{3} \frac{w_1}{e z_{max}} \ . \tag{76}$$

The surface charge density is

$$\sigma = \sqrt{m r_0 v_1 / \pi} \ , \tag{77}$$

and the total number of electrons is

$$N_s = \frac{\sigma}{e} = \sqrt{\frac{m r_0 v_1}{\pi e^2}} = 3\, n(0)\, z_{max} \left(\frac{\text{elecs}}{\text{cm}^2} \right) \ . \tag{78}$$

The number density is

$$n(z) = n(0)\ (1 - z/z_{max})^{-2/3} \ , \tag{79}$$

and diverges as $z \to z_{max}$. The electric field and potential are

$$E(z) = E(0)\ (1 - z/z_{max})^{1/3} \ , \tag{80}$$

$$\Phi(z) = \frac{w_1}{e} \left[(1 - z/z_{max})^{4/3} - 1 \right] \ . \tag{81}$$

and the dipole moment is

$$P = \frac{w_1}{4\pi e} = \frac{3}{4}\, e N_s z_{max} \qquad \text{esu/cm} \ . \tag{82}$$

The stored kinetic energy is

$$K = \frac{1}{5}\, w_1 N_s \ , \tag{83}$$

and the stored electrostatic energy is

$$U_E = 2\ K \ , \tag{84}$$

since there is no x or y motion.

The time for an electron to reach z_{max} is

$$t_{max} = \frac{3\, z_{max}}{v_1} = \sqrt{\frac{m v_1}{4\pi e^2 r_0}} \ . \tag{85}$$

An electron's trajectory is

$$v(t) = v_1(1 - t/t_{max})^2 \quad 0 < t < t_{max} , \tag{86}$$

$$z(t) = z_{max}[1 - (1 - t/t_{max})^3] \quad 0 < t < t_{max} , \tag{87}$$

and

$$v(z) = v_1(1 - z/z_{max})^{2/3} . \tag{88}$$

An electron leaving the surface sees an electric field decreasing linearly with time.

The number density $n(z)/n(0)$ and electric field $E(z)/E(0)$ normalized to their value at $z = 0$ are shown as curve 1 in Figures 3 and 4. The normalized potential, $-e\Phi/w_1$, is shown as curve 1 in Figure 5.

Example 2 - $\cos\theta$ angular distribution, monoenergetic energy distribution (case 1 of Section 3). This is the same as a normal emission, constant spectrum, and was discussed by Hale[2]. Here

$$\frac{dn}{dw} = r_0\delta(w - w_1) ,$$

and, with $v_1 = \sqrt{2w_1/m}$, we find

$$n(0) = \frac{4r_0}{v_1} , \tag{89}$$

$$\ell_D = \sqrt{\frac{w_1 v_1}{16\pi e^2 r_0}} , \tag{90}$$

$$z_{max} = 2\sqrt{3}\,\ell_D , \tag{91}$$

$$E(0) = 4\sqrt{2\pi m r_0 v_1/3}$$

$$= 4\,\frac{w_1}{e z_{max}} , \tag{92}$$

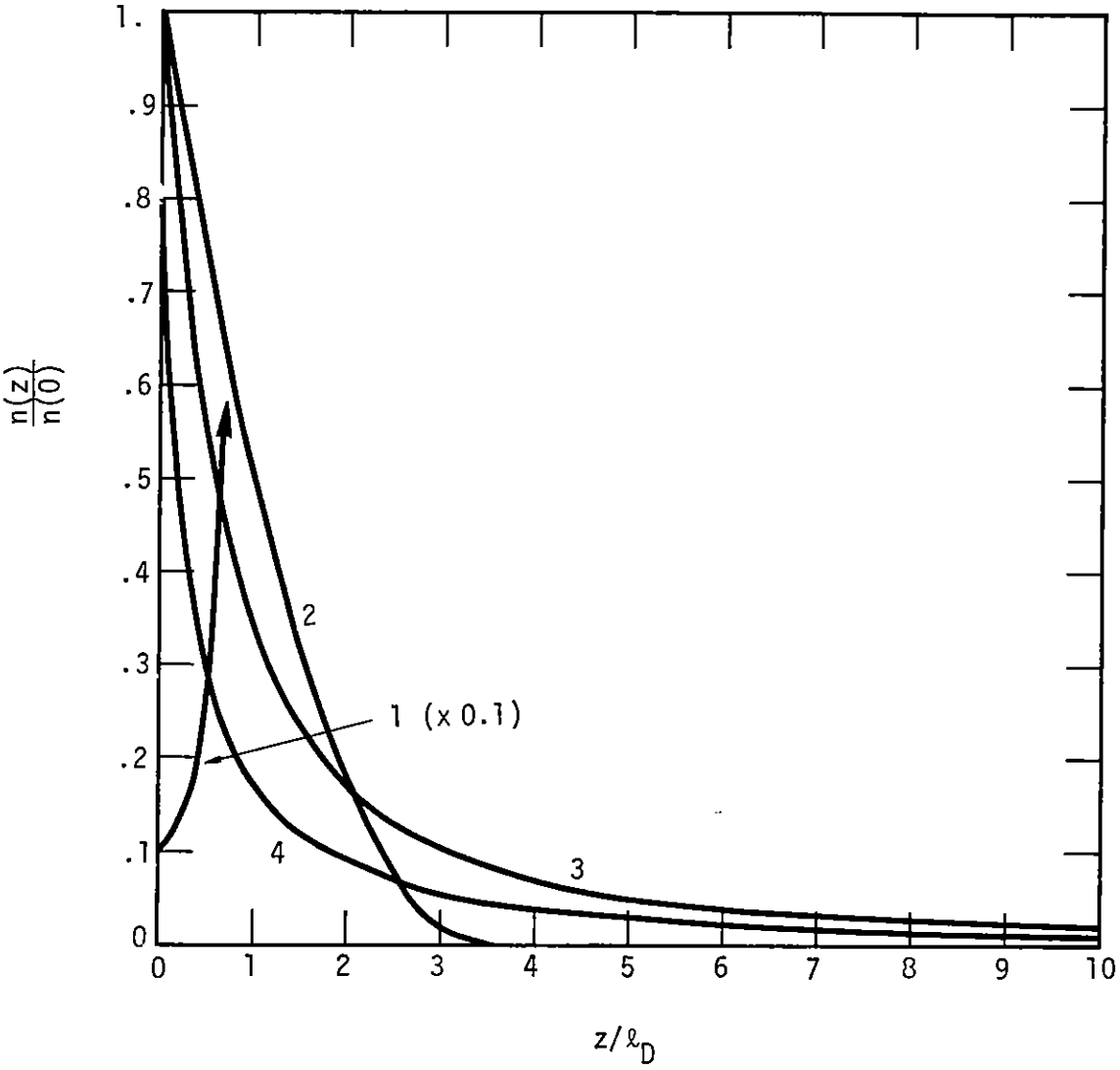

Figure 3. Normalized electron number density vs. distance from surface.

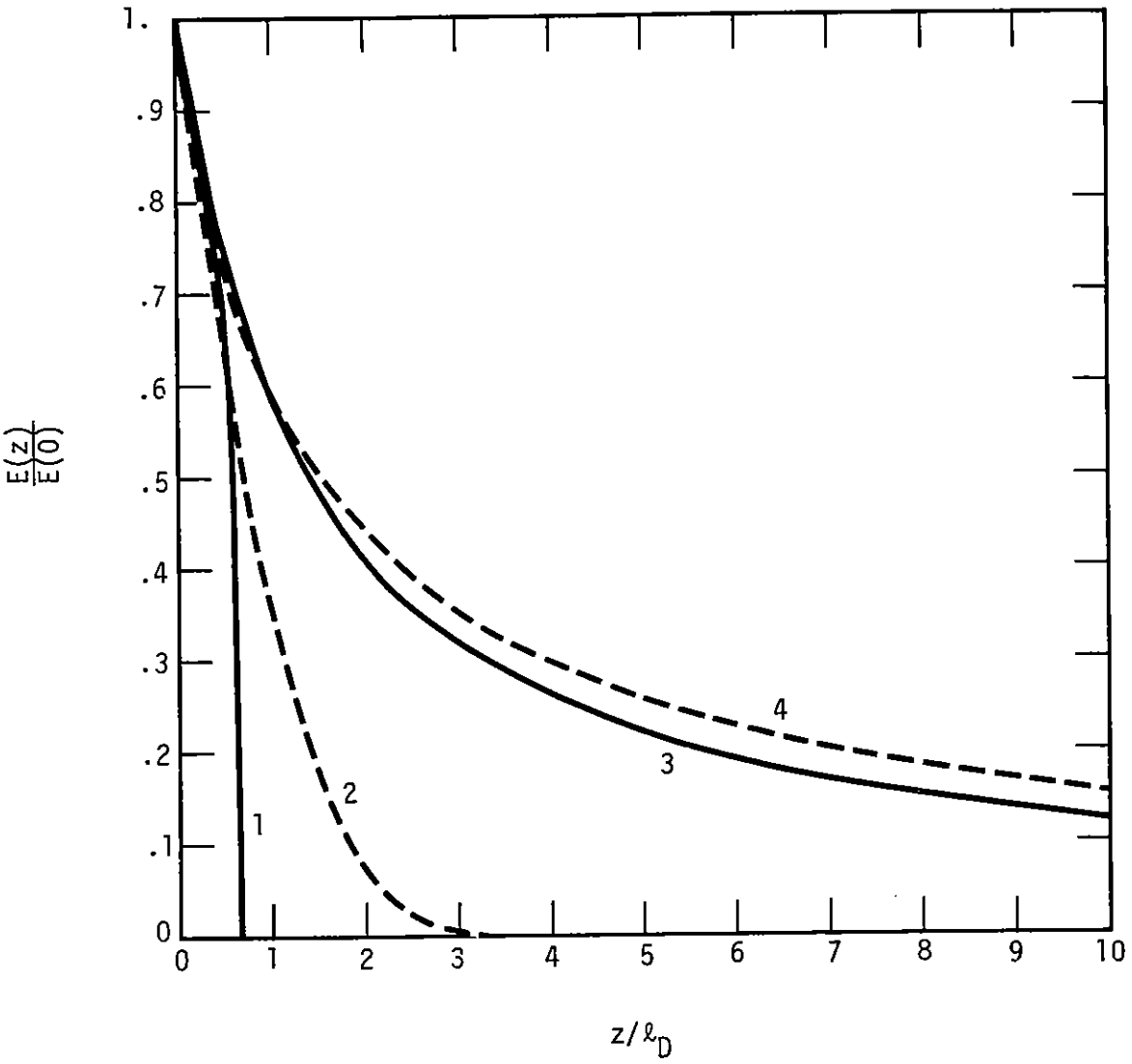

Figure 4. Normalized electric field vs. distance from surface.

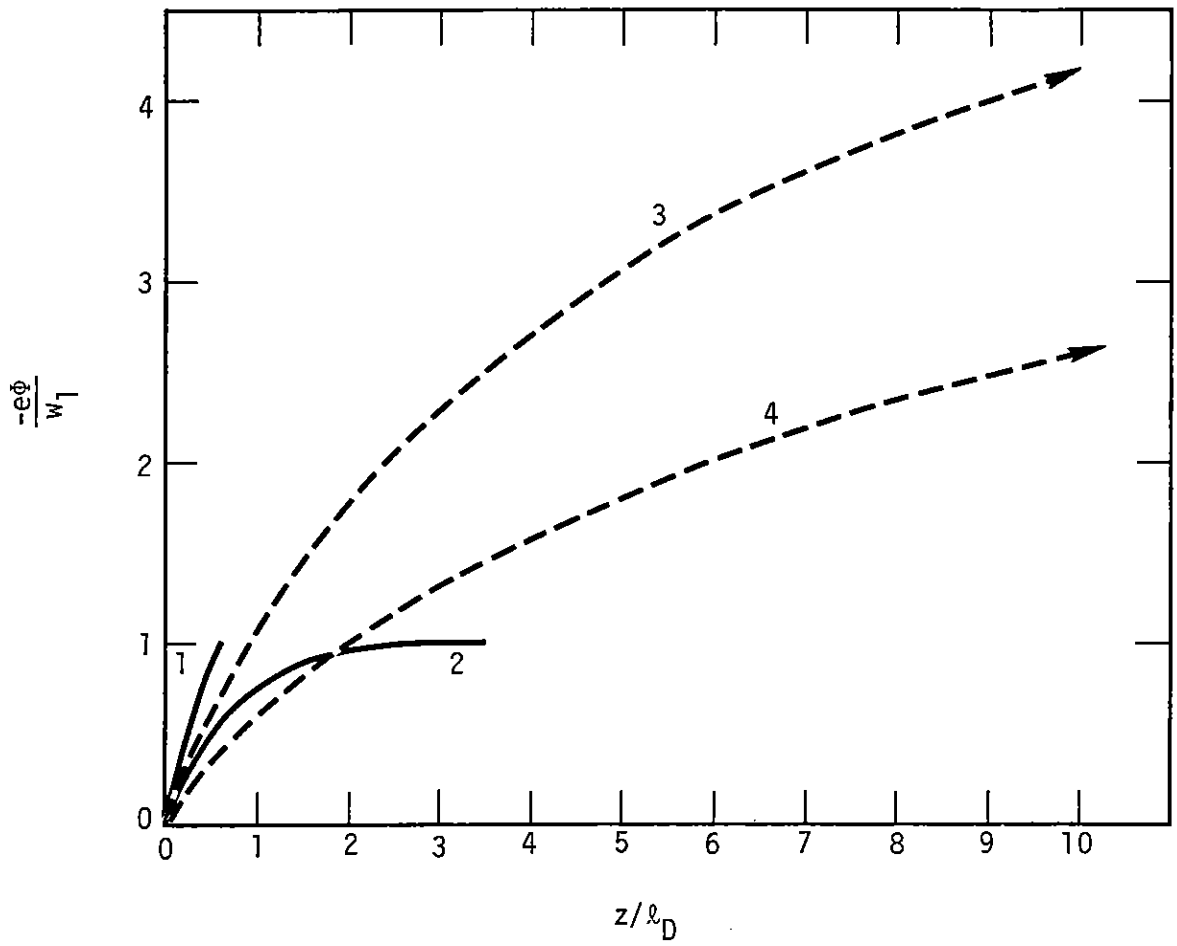

Figure 5. Normalized potential vs. distance from surface.

$$\sigma = \sqrt{2mr_0 v_1/3\pi} \ , \tag{93}$$

$$N_s = \frac{\sigma}{e} = \frac{1}{3}\, n(0) z_{max} \ , \tag{94}$$

$$n(z) = n(0)\ (1 - z/z_{max})^2 \ , \tag{95}$$

$$E(z) = E(0)\ (1 - z/z_{max})^3 \ , \tag{96}$$

$$\Phi(z) = \frac{w_1}{e}\ [(1 - z/z_{max})^4 - 1] \ , \tag{97}$$

$$P = \frac{w_1}{4\pi e} = \frac{1}{4}\, eN_s z_{max} \ , \tag{98}$$

$$K_z = \frac{1}{7}\, w_1 N_s \ , \tag{99}$$

$$U_E = 2\, K_z = \frac{2}{3}\, K \ , \tag{100}$$

$$v(z) = v_1 (1 - z/z_{max})^2 \ . \tag{101}$$

The maximum distance $z_{max}(w_z)$ an electron with z component of energy w_z, $0 < w_z < w_1$, will go is

$$z_{max}(w_z) = z_{max}[1 - (1 - w_z/w_1)^{1/4}] \ . \tag{102}$$

Trajectories and turn around times involve elliptic functions, but in the case of a particle emitted with energy $w_z = w_1/2$, we find

$$t_{max}(w_z = \frac{1}{2}\, w_1) \approx 0.49\ \frac{z_{max}}{v_1} \ . \tag{103}$$

The number density, electric field, and potential are plotted as curve 2 in Figures 3, 4, and 5.

Example 3 - $\cos\theta$ angular distribution, linear times exponential energy distribution (case 6 of Section 3). In this example the integrals in Equations 57 and 58 can be done analytically.

$$\frac{dn}{dw} = \frac{r_0}{w_1^2} w\, e^{-w/w_1}$$

$$v_1 = \sqrt{2w_1/m} .$$

We find

$$n(0) = 2\sqrt{\pi}\, \frac{r_0}{v_1} , \tag{104}$$

$$\ell_D = \sqrt{\frac{w_1 v_1}{8\pi^{3/2} e^2 r_0}} . \tag{105}$$

Define

$$\ell_1 = \sqrt{2}\, \ell_D ,$$

which is the Debye length at the surface of the electrons which are leaving the surface. Then

$$E(0) = \sqrt{8\pi^{3/2} m r_0 v_1}$$

$$= \frac{2w_1}{e\ell_1} , \tag{106}$$

$$\sigma = \sqrt{m r_0 v_1 / 2\sqrt{\pi}} , \tag{107}$$

$$N_s = \frac{\sigma}{e} = n(0)\ell_1 , \tag{108}$$

$$n(z) = n(0)\ (1 + z/\ell_1)^{-2} , \tag{109}$$

$$E(z) = E(0)\ (1 + z/\ell_1)^{-1} , \tag{110}$$

$$\Phi(z) = -\frac{2w_1}{e} \ell n\ (1 + z/\ell_1)\ , \tag{111}$$

$$K_z = \frac{1}{2} w_1 N_s\ , \tag{112}$$

$$U_E = 2\,K_z = \frac{2}{3} K\ . \tag{113}$$

The dipole moment per unit area due to electrons out to z is

$$P(z) = \frac{w_1}{2\pi e}\left[\ell n(1 + z/\ell_1) - \frac{z}{z + \ell_1}\right]\ . \tag{114}$$

For $z >> \ell_1$ this depends only logarithmically on the fluence through ℓ_1.

An electron emitted with velocity v and energy $w = \frac{1}{2} mv^2$ has velocity

$$v(z) = v\left[1 - 2\,\frac{w_1}{w}\,\ell n(1 + z/\ell_1)\right]^{1/2}\ , \tag{115}$$

and reaches maximum distance

$$z_{max}(v) = \ell_1\left(e^{w/2w_1} - 1\right)\ , \tag{116}$$

in a time

$$t_{max}(v) = \sqrt{\frac{\pi}{2}}\,\frac{\ell_1}{v_1}\,e^{w/2w_1}\,\mathrm{erf}(v/\sqrt{2}\,v_1)\ , \tag{117}$$

where erf(x) is the error function. For $v = v_1$,

$$t_{max}(v_1) \approx 1.405\,\frac{\ell_1}{v_1}\ . \tag{118}$$

Figures 3, 4, and 5 show n(z), E(z), and $\Phi(z)$ in curve 3.

Example 4 - $\cos\theta$ angular distribution, exponential energy distribution (case 5 of Section 3). This distribution corresponds closely with the experimental distributions for blackbody photon sources. The complete solution cannot be obtained in closed form.

$$\frac{dn}{dw} = \frac{r_0}{w_1} e^{-w/w_1}$$

$$v_1 = \sqrt{2w_1/m} .$$

We find

$$n(0) = 4\sqrt{\pi}\,\frac{r_0}{v_1} , \tag{119}$$

$$\ell_D = \sqrt{\frac{w_1 v_1}{16\pi^{3/2} e^2 r_0}} , \tag{120}$$

$$E(0) = \sqrt{16\pi^{3/2} m r_0 v_1/3} , \tag{121}$$

$$\sigma = \sqrt{m r_0 v_1/3\sqrt{\pi}} , \tag{122}$$

$$N_s = \sqrt{\frac{m r_0 v_1}{3\sqrt{\pi} e^2}} = \sqrt{\frac{2}{3}}\, n(0)\ell_D . \tag{123}$$

As a function of the dimensionless potential

$$\psi = \frac{-e\Phi(z)}{w_1} , \tag{124}$$

the number density and electric field are

$$n = n(0)[e^{-\psi} - \sqrt{\pi}\sqrt{\psi}\,\mathrm{erfc}(\sqrt{\psi})] . \tag{125}$$

$$E = E(0)[(1 - 2\psi)e^{-\psi} + 2\sqrt{\pi}\psi^{3/2}\,\mathrm{erfc}(\sqrt{\psi})]^{1/2} . \tag{126}$$

The inverse of $\psi(z)$ is

$$z = \sqrt{\frac{3}{2}}\,\ell_D \int_0^{\psi} d\psi\left[(1 - 2\psi)e^{-\psi} + 2\sqrt{\pi}\psi^{3/2}\ \mathrm{erfc}(\sqrt{\psi})\right]^{-1/2} \quad (127)$$

Here, erfc(x) is the complementary error function 1 - erf(x). Figures 3, 4, and 5 show n(z)/n(0), E(z)/E(0), and $\psi(z)$ obtained from a numerical evaluation of Equations 125 through 127. The abscissae in Figures 3, 4, and 5 are scaled to the Debye lengths Equations 74, 90, 105, or 120, appropriate to each example.

The asymptotic behaviors are

$$n(z) \xrightarrow{z \to \infty} n(0)\ \frac{2\ell_D^2}{z^2}\ , \quad (128)$$

$$E(z) \xrightarrow{z \to \infty} E(0)\ \frac{\sqrt{6}\ell_D}{z}\ , \quad (129)$$

$$\psi e^{\psi} \xrightarrow{z \to \infty} \frac{z^2}{4\ell_D^2}\ , \quad (130)$$

so that Φ diverges logarithmically. For $z \ll \ell_D$ we find

$$n(z) \to n(0)\left[1 - 1.602\sqrt{\frac{z}{\ell_D}}\right]\ , \quad (131)$$

$$E(z) \to E(0)\left[1 - \sqrt{\frac{3}{2}}\frac{z}{\ell_D}\right]\ , \quad (132)$$

$$\psi(z) \to \sqrt{\frac{2}{3}}\frac{z}{\ell_D}\ , \quad (133)$$

so that dn(z)/dz diverges at the surface.

The dipole moment, Equation 62, diverges logarithmically with Φ and is only weakly dependent on fluence, as was the case in Example 3. P(z) vs. z is shown in Figure 6.

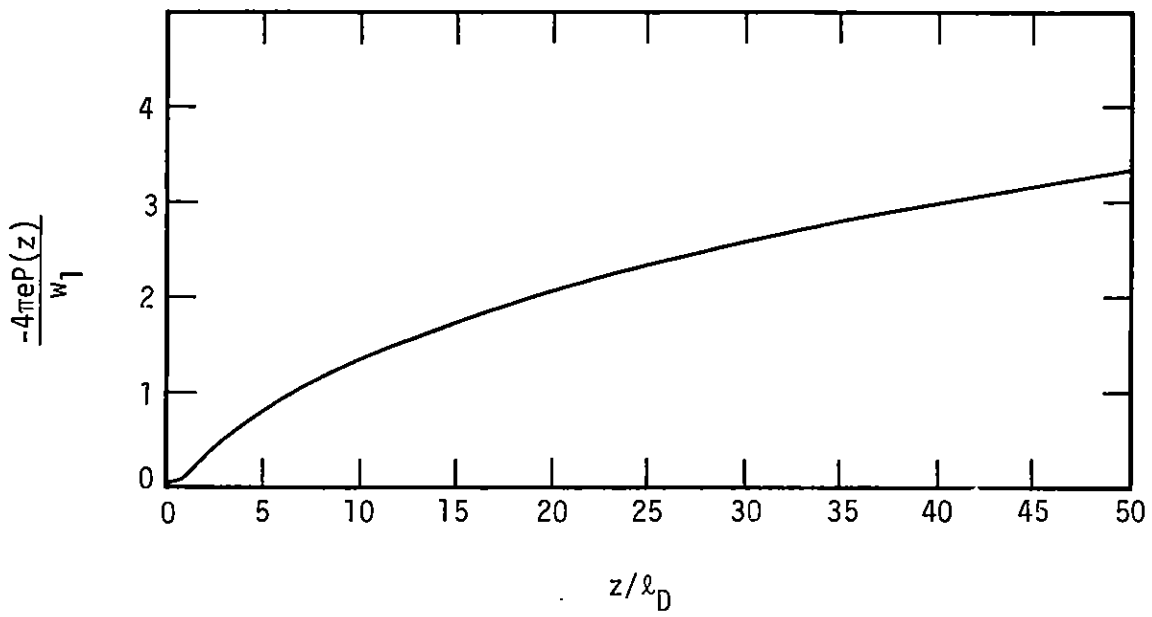

Figure 6. Dipole moment vs. distance from surface.

An electron ejected with z component of velocity v_{z0} and $w_z(0) = \frac{1}{2} m v_{z0}^2$ has z component of kinetic energy at z given by

$$w_z(z) = w_z(0) + e\Phi(z) \ , \qquad (134)$$

which is shown in Figure 7 for several values of $w_z(0)$, showing how various particles slow down with distance from the surface. The maximum distance such a particle will go, $z_{max}(w_z(0))$, and the time $t_{max}(w_z(0))$ to reach this distance are shown in Figure 8. Particles ejected with $w_z < w_1$ go less than two Debye lengths.

The total stored kinetic energy is

$$K = 3\ K_z$$
$$= 1.012\ w_1 N_s \ , \qquad (135)$$

where K_z is the total kinetic energy stored in the z component of motion, and the energy in the electric field, U_E, is 2K/3 in accordance with Section 6.

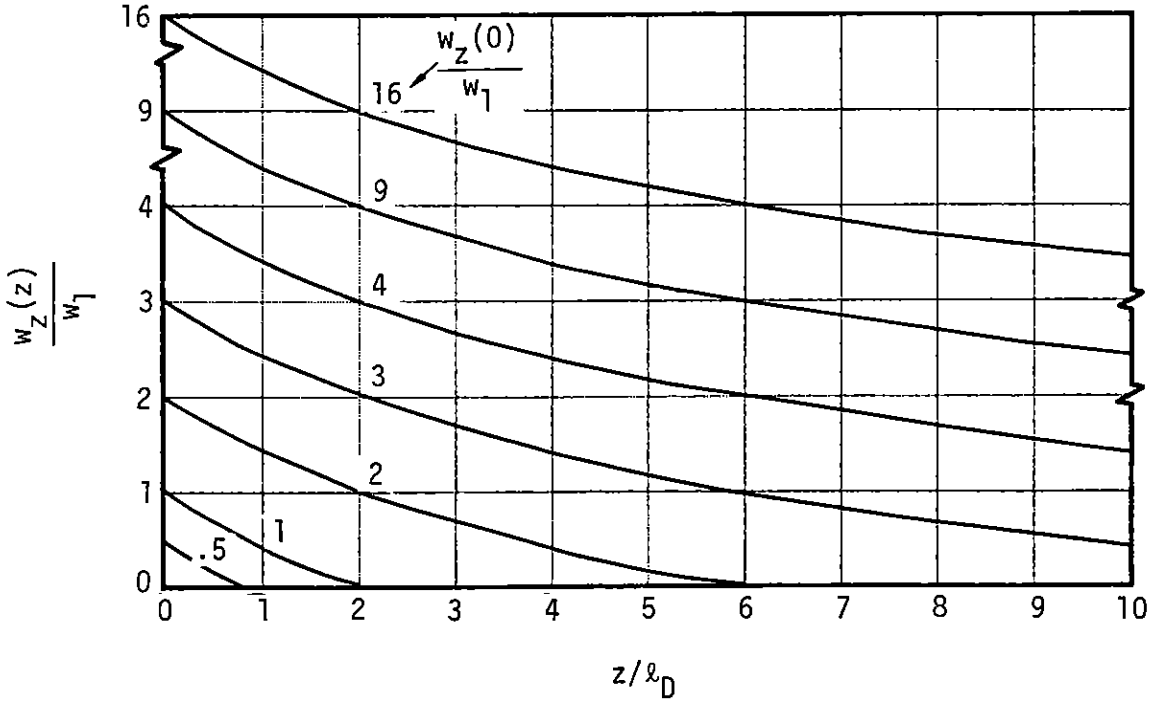

Figure 7. z component of kinetic energy vs. distance from surface.

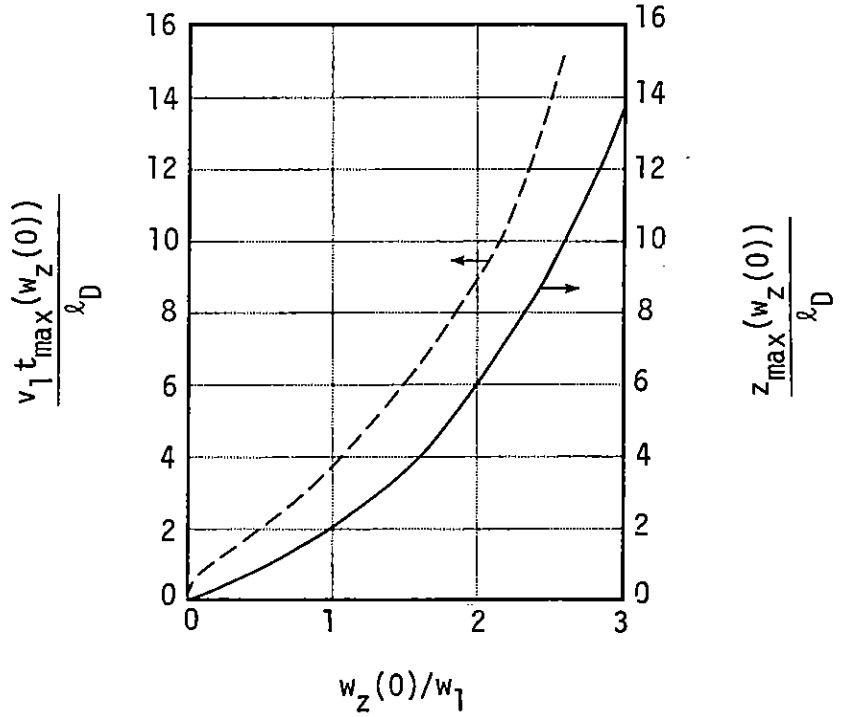

Figure 8. z_{max} and t_{max} as a function of normal emission energy.

Values of the Debye lengths, Equation 120, are given in Reference 4.

Referring to Figure 3, we see that in this example the number density drops off very rapidly at first, falling to half its surface value in less than 1/4 Debye length. Both of the finite energy spectra, Examples 1 and 2, give a very poor representation of the electron density. In Example 3 the absence of the low-energy electrons causes the density to drop off more slowly than in Example 4.

The low-energy electrons double the surface value of n, Equations 104 and 119. The electric fields have a very similar behavior as seen in curves 3 and 4 in Figure 4.

In Example 4, Figure 6 shows that the dipole moment varies slowly with distance, remaining of order $w_1/4\pi e$ for many Debye lengths. But at one Debye length it is only 0.11 $w_1/4\pi e$.

SECTION 8

SUMMARY

We have presented the solution of the steady-state one-dimensional boundary layer problem, summarizing previous work and presenting the solution for the interesting exponential energy spectrum in some detail.

In general we find both the electron number density at the surface and the surface charge density (and also, therefore, the electric field at the surface) are independent of the electron charge. The characteristic potential of the layer and the dipole moment per unit area depend only weakly on the fluence in the case of an exponential energy spectrum. General principles imply that the energy stored in the electric field is just twice that stored in the kinetic energy of the normal component of motion.

Estimates for the times at which the steady-state solution should apply show it to be valid if the X-ray flux changes only slightly in about 1 nanosec for fluences above 10^{-3} cal/cm^2.

REFERENCES

1. Karzas, W. J., and R. Latter, "Electromagnetic Radiation from a Nuclear Explosion in Space," Phys. Rev., 126, pp. 1919-1926, June 1962 (EMP Theoretical Note 27).

2. Hale, C. R., Electric Fields Produced by an Electronic Current Emitted Perpendicular to a Surface, Air Force Weapons Laboratory, EMP Theoretical Note 115, April 1971.

3. Higgins, D. F., Highly Space Charge Limited SGEMP Calculations, Mission Research Corporation, unpublished.

4. Carron, N. J., Characteristic Steady-State Electron Emission Properties for Parametric Blackbody X-ray Spectra on Several Materials, Mission Research Corporation, MRC-N-221, DNA 3931T, February 1976.

5. Longmire, C. L., Elementary Plasma Physics, John Wiley, Interscience, New York, 1963, Chapter 1.